Journal of Computational Physics 298 (2015) 266–279

Contents lists available at ScienceDirect

Journal of Computational Physics

www.elsevier.com/locate/jcp

A method for spectral DNS of low *Rm* channel flows based on the least dissipative modes

Kacper Kornet *, Alban Pothérat

Applied Mathematics Research Centre, Coventry University, Priory street, Coventry CV1 5FB, UK

ARTICLE INFO

Article history:
Received 9 December 2013
Received in revised form 8 May 2015
Accepted 14 May 2015
Available online 19 May 2015

Keywords:
Spectral methods
Low *Rm* MHD

ABSTRACT

We put forward a new type of spectral method for the direct numerical simulation of flows where anisotropy or very fine boundary layers are present. The main idea is to take advantage of the fact that such structures are dissipative and that their presence should reduce the number of degrees of freedom of the flow, when paradoxically, their fine resolution incurs extra computational cost in most current methods. The principle of this method is to use a functional basis with elements that already include these fine structures so as to avoid these extra costs. This leads us to develop an algorithm to implement a spectral method for arbitrary functional bases, and in particular, non-orthogonal ones. We construct a basic implementation of this algorithm to simulate magnetohydrodynamic (MHD) channel flows with an externally imposed, transverse magnetic field, where very thin boundary layers are known to develop along the channel walls. In this case, the sought functional basis can be built out of the eigenfunctions of the dissipation operator, which incorporate these boundary layers, and it turns out to be non-orthogonal. We validate this new scheme against numerical simulations of freely decaying MHD turbulence based on a finite volume code and it is found to provide accurate results. Its ability to fully resolve wall-bounded turbulence with a number of modes close to that required by the dynamics is demonstrated on a simple example. This opens the way to full-blown simulations of MHD turbulence under very high magnetic fields. Until now such simulations were too computationally expensive. In contrast to traditional methods the computational cost of the proposed method, does not depend on the intensity of the magnetic field.

1. Introduction

In the field of numerical simulations of fluid flows, spectral methods present well established advantages in terms of precision and resolution over classical mesh-based methods such as finite differences, finite elements or finite volumes methods. On the flip side, they are only well developed and widely used for a limited set of functional bases (such as Fourier bases), and therefore tend to be limited to ideal geometries. Difficulties start appearing as soon as bounding walls are present: in a channel bounded by two parallel walls, Tchebychev polynomials are used in the transverse direction that present the same advantages as Fourier modes in periodic domains (orthogonality in both continuous and discrete physical domains, fast forward and inverse transforms between real and spectral spaces available to calculate non-linear terms, and exponential convergence). They are particularly well suited to satisfy no-slip boundary conditions at the wall

* Corresponding author.
E-mail address: kk562@cam.ac.uk (K. Kornet).

http://dx.doi.org/10.1016/j.jcp.2015.05.018
0021-9991/

because the locus of their zeros, used as collocation points, are all the more concentrated near the walls as their order is high. This property, most welcome to resolve strong velocity gradients of wall boundary layers, is also their downfall. When the boundary layers become very thin, the number of basis elements required to resolve them becomes very large. Furthermore, the spatial distribution of the collocation points being highly inhomogeneous, the high resolution required to resolve fine turbulent structures in the bulk implies a large number of unnecessary collocations points near walls. Not only does this result in high computational costs but it also brings concerns about the accuracy of the obtained results, as the linear systems needed to be solved become more and more ill-conditioned with increasing number of used modes. One such example is found in flows of liquid metals under high magnetic fields (such as in the cooling blankets of ITER, the future nuclear fusion reactor [1]). The corresponding idealised configuration is that of a liquid metal channel flow (height $h \sim 10$ cm) placed in a homogeneous static transverse magnetic field $B \sim 10$ T: Hartmann wall boundary layers are known to develop and their thickness scales as $\delta \sim h\sqrt{\rho\nu/\sigma}/B$. For a typical liquid metal of conductivity $\sigma \simeq 10^6$ S/m, density $\rho \sim 10^4$ kg/m^3 and kinematic viscosity $\nu \sim 10^{-7}$ m^2/s, $\delta \sim 10^{-7}$–10^{-6} m. Zeroes of Tchebychev polynomials of order n are spaced by a distance scaling as n^{-2} near the wall. Consequently, the number of Tchebychev polynomials required to resolve such a flow scales with the square root of Hartmann number $\sqrt{Ha} \sim \sqrt{h/\delta}$, and demands unrealistic computational power [2]. Yet, the enormous dissipation incurred by friction and Joule dissipation in these layers decimates the degree of freedom of the flow when Ha becomes large. Their number can be estimated through the dimension d_M of the attractor of the underlying system, for which an upper bound was shown to scale as Ha^{-1} [3]. The fact that the number of modes needed to resolve the flow completely increases in numerical simulations at high Ha is therefore a property of the spectral method based on these polynomials, but does not reflect any physical constraint.

An "ideal" spectral method would only require a number of modes of the order of the attractor dimension, which would be achieved by using a functional basis spanning the smallest linear space that embeds the attractor. Finding such basis in complex geometries is unfortunately not a realistic task. Ref. [3], however, proved that in the case of the MHD channel flow, the basis of eigenmodes of the linear part of Navier–Stokes equations spanned a space in which any d_M-dimensional volume of initial conditions contracted to 0 through the governing equations. From the physical point of view, these modes were shown to exhibit numerous properties of the actual MHD channel flow: same anisotropy and, especially, their profile across the channel includes that of a Hartmann layer, so representing these layers using this basis only requires a small number of modes.

This paper explores the idea of building a numerical spectral code based on this "dynamically relevant" functional basis. Expansions over eigenbases of linear operators have been commonly used to solve viscous flows [4] and other problems involving the Laplacian operator. Some problems also require tailored functional bases to deal with specific geometries and boundary conditions: in the context of geophysical flows, [5] put forward a basis to circumvent difficulties arising from the singularities of spherical harmonics at the centre of a spherical domain. The novelty here is to apply this technique to highly non-linear problems in the hope of keeping the number of modes required for full resolution close to that strictly required by the dynamics of the system. Since current spectral codes rely on a number of favourable properties of classical Fourier or Tchebychev bases (orthogonality, fast transforms), building a new code for arbitrary functional bases poses a number of problems, particularly in dealing with the non-linear part of the Navier–Stokes equations. The absence of these features makes the implementation more difficult and adversely affects performance. Nevertheless, the challenge of using dynamically relevant bases is to outweigh this loss by using significantly less modes. For MHD channel flows, this strategy is expected to become advantageous at high Ha. Therefore, the purpose of the present paper is to demonstrate an implementation of this method for MHD channel flows, to show that the resulting code provides accurate results and also that it makes it possible to simulate regimes of very high magnetic fields otherwise not accessible. The emphasis is laid on the generality of this implementation, rather than performance optimisation. The code we shall describe can be used with a large variety of other functional bases associated to different geometries and boundary conditions.

The governing equations for the MHD channel flow and the associated functional base are presented in Section 2. The numerical method is described in Section 3. Finally, the code is tested in Section 4, where its ability to resolve freely decaying turbulence in an MHD channel is compared to that of a finite volume code. We also show on an example that flows at high Hartmann numbers can be resolved with limited computational power.

2. Governing equations and their properties

2.1. The low-Rm MHD equations

Flows of liquid metals in engineering applications are usually described within the frame of the Low Magnetic Reynolds number (Rm) approximation. This applies to problems where the flow is neither intense nor conductive enough to induce a magnetic field comparable to an externally applied one. The full system of the induction equation and the Navier–Stokes equations for an incompressible fluid are then approximated to the first order in Rm, which represents the ratio of these two fields. This leads to the following system [6]:

$$\frac{\partial \mathbf{u}}{\partial t} + (\mathbf{u}\cdot\nabla)\mathbf{u} = -\frac{1}{\rho}\nabla p + \nu\Delta\mathbf{u} + \frac{1}{\rho}\mathbf{j}\times\mathbf{B}, \tag{1}$$

$$\nabla\cdot\mathbf{u} = 0, \tag{2}$$

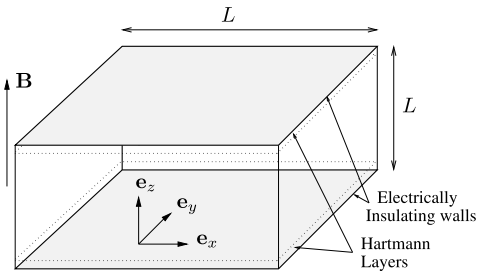

Fig. 1. Geometry of the channel flow with transverse magnetic field.

$$\nabla \cdot \mathbf{j} = 0\,, \tag{3}$$

$$\mathbf{j} = \sigma(-\nabla\Phi + \mathbf{u}\times\mathbf{B})\,, \tag{4}$$

where $\mathbf{u}$ denotes fluid velocity, $\mathbf{B}$ – magnetic field, $\mathbf{j}$ – electric current density, ν – kinematic viscosity, σ – electrical conductivity, Φ – electric potential. We consider a channel flow with a homogeneous transverse magnetic field $B\mathbf{e}_z$ and impermeable ($\mathbf{u}|_{wall} = \mathbf{0}$), electrically insulating ($\mathbf{j}\cdot\mathbf{n}|_{wall} = \mathbf{0}$) walls located at $z = \pm L/2$. In the xy directions we adopt the periodic boundary conditions with period L (see Fig. 1). Under this assumptions and using the reference scale L, time L^2/ν and velocity ν/L the above set of equations can be expressed in dimensionless form:

$$\frac{\partial \mathbf{u}}{\partial t} + P(\mathbf{u}\cdot\nabla)\mathbf{u} = \Delta\mathbf{u} - Ha^2\Delta^{-1}\partial_{zz}\mathbf{u}\,, \tag{5}$$

where $Ha = LB\sqrt{\sigma/\rho\nu}$ is the Hartman number and P denotes orthogonal projection onto the subspace of solenoidal fields. $\Delta^{-1}\partial_{zz}\mathbf{u}$ is defined as a vector field $\mathbf{w}$ which is a solution to equation:

$$\Delta\mathbf{w} = \partial_{zz}\mathbf{u}\,.$$

The boundary conditions necessary to solve the above equation are derived from the boundary condition for the velocity and current density. Even though ν/L provides a natural scale for velocity, actual velocities, particularly in turbulence flows are most of the time significantly higher. If U_0 is their typical scale, the Reynolds number $U_0 L/\nu$ provides a measure of the intensity of turbulence.

2.2. Eigenvalue problem for the dissipation operator

In [7], a set of solenoidal solutions to eigenvalue problem of the operator $\mathcal{L}$ that represents the linear part of eq. (5):

$$\mathcal{D}_{Ha}\mathbf{u} = -Ha^2\Delta^{-1}\partial_{zz}\mathbf{u} + \Delta\mathbf{u} = \lambda\mathbf{u}\,, \tag{6}$$

$$\nabla\cdot\mathbf{u} = 0 \tag{7}$$

together with the problem's boundary conditions, was derived (for their full form see Appendix A). The features of flows at high Ha are strongly determined by the properties of this operator. Because of this, the set of modes built out of its eigenfunctions elements includes structures that are actually present in the flow. Laminar and turbulent Hartmann boundary layers that develop along the channel walls appear, in particular, as built-in features of these modes [7,8]. They are therefore natural candidates to be used as elements of a functional basis in a numerical spectral scheme. Moreover, these modes all have negative eigenvalues, and it can be shown that to resolve the flow completely, it is only necessary to take into account all modes with eigenvalue λ with a modulus below a maximum $|\lambda_{\max}|$, such that their total number scales as Re^2/Ha [3]. Since the operator defined in (6) represents the sum of viscous and Joule dissipation, the set of modes defined in this way is in fact the set of *least dissipative modes*. For sufficiently large values of Ha, this number becomes significantly smaller than the number of Fourier or Tchebychev modes necessary to resolve the Hartmann layers [7]. However, there are also some disadvantages in using these alternative modes. The main complication comes lies in the calculation of nonlinear terms. In standard spectral schemes using an orthogonal basis, these are first "transformed back" to be expressed in terms of physical coordinates (x, y, z). The non-linear terms are then calculated in this expansion and subsequently their spectral expansion is found by calculating their scalar products with each of the basis elements. The last step uses the orthogonality of the modes. The eigenbasis of $\mathcal{D}_{Ha}$, by contrast, is not orthogonal. In theory, projection can still be performed without an orthogonal basis, using the basis of eigenfunctions and associate eigenfunctions of the adjoint operator. The latter may, however, be difficult to express explicitly, as in the present case. Therefore we chose to develop an alternative procedure for projection of non-linear terms on the space spanned by these modes, which we shall now describe. A significant advantage of using a decomposition over the eigenmodes of $\mathcal{D}_{Ha}$ is that since these modes satisfy (2) and (3), the solution conserves mass and charge to the precision of the truncation error by construction (throughout the paper, we will refer to this level of precision as "exact" in the sense that it involves no error originating from the algorithm). Conservation of charge is particularly crucial in problems with electrically insulating boundaries, where eddy currents must close withing the fluid

domain. Failure to ensure it to the precision of the algorithm results in numerical instability and/or significant errors in the final solution, as proved by [9] for codes based on the finite volume method. In such codes, dedicated algorithms have to be designed to take care of this particular difficulty that can incur extra computational cost (see [10]).

3. Method

Given a complete set of basis functions spanning a space of solutions to the considered equations, any velocity field can be expressed in two ways. In the first one, it is expressed as a function of coordinates (x, y, z). In the second one, which we call a spectral expansion, it is expressed as a series over the set of basis functions. The idea behind spectral methods is to search for a solution of the governing equations in its spectral expansion. Our aim is to use a basis consisting of functions that are better suited for the considered physical flow than the usually adopted Fourier or Tchebychev expansions. Namely, for our basis we use the least dissipative modes introduced in Section 2.2. Since the non-linear terms do not preserve the divergence-free property, the solenoidal modes have to be complemented by additional non-solenoidal basis elements satisfying the boundary conditions. By virtue of the existence and uniqueness of the Helmholtz decomposition, it suffices to supplement the original basis with additional elements spanning the subspace of irrotational functions. In the particular case of low Rm channel configuration, these are obtained by solving the eigenvalue problem (6), with condition (7) replaced with $\nabla \times \mathbf{u} = 0$, again with the problem's boundary conditions. Their full form can be found in Appendix A.

3.1. Discretisation

As mentioned in Section 2.2, the non-linear terms cannot be treated under their expanded form, or at least, the costs of doing so would be prohibitive [11]. Instead, they should be dealt with in the physical space, and this requires to know their value in a discrete number of points. For this, we start from the more general form of eq. (5):

$$\dot{\mathbf{u}}(t, \mathbf{x}) + \mathcal{D}_{Ha}(\mathbf{u}(t, \mathbf{x})) = P(G(\mathbf{u}(t, \mathbf{x}))) \,, \tag{8}$$

with appropriate boundary conditions. $\mathcal{D}_{Ha}$ is here a linear operator and G includes the nonlinear terms. In this section we provide a general method to solve this type of equations on a set of discrete points $\{\mathbf{x}_i\} = \{(x_i, y_i, z_i)\}$. The method does not depend on specific locations of $\{\mathbf{x}_i\}$. Therefore we shall not specify them at this point, but only later when the method is applied to the specific problem of MHD channel flows. We first rewrite eq. (8) in the weak form:

$$\langle \dot{\mathbf{u}}(t, \mathbf{x}) + \mathcal{D}_{Ha}(\mathbf{u}(t, \mathbf{x})), \mathbf{v} \rangle = \langle P(G(\mathbf{u}(t, \mathbf{x}))), \mathbf{v} \rangle \,, \tag{9}$$

where $\{\mathbf{v}\}$ is a set of test functions and $\langle \cdot | \cdot \rangle$ is the scalar product associated to the $\mathcal{L}_2$ norm. As we are using a spectral approach to solve (8), the solution is expressed as a series:

$$\mathbf{u}(t, \mathbf{x}) = \sum_n a_n(t) \mathbf{e}_n(\mathbf{x}) \,, \tag{10}$$

where $\{\mathbf{e}_n(\mathbf{x})\}$ is a functional basis, here chosen among eigenfunctions of $\mathcal{D}_{Ha}$. In the particular case of channel flows in low Rm approximation $\{\mathbf{e}_n(\mathbf{x})\} = \mathbf{e}_{\{k_x, k_y, q, i\}}$, where $\mathbf{k}_\perp = [k_x, k_y]$ is a wave vector in the plane parallel to the walls, $q \in \mathbb{N}$ and $i = 1, 2, 3, 4, 5, 6$. We provide their explicit forms in the Appendix A. If we choose as trial functions the set of Dirac-delta functions located at points $\{x_i\}$, insert expression (10) into equation (9), and use the fact that $\mathbf{e}_n(\mathbf{x})$ are eigenvectors of operator $\mathcal{D}_{Ha}$, we obtain a set of equations:

$$\sum_n \dot{a}_n(t) \mathbf{e}_n(\mathbf{x}_i) + a_n(t) \lambda_n \mathbf{e}_n(\mathbf{x}_i) = P(G(\mathbf{u}(t, \mathbf{x}_i))) \,, \tag{11}$$

where λ_n is the eigenvalue associated to $\mathbf{e}_n$. Further we assume that the set of eigenfunctions can be divided into two subsets. One consisting of solenoidal modes and the other consisting of irrotational modes. Then if we express the non-linear terms in the same basis,

$$G(\mathbf{u}(t, \mathbf{x}_i)) = \sum_n g_n \mathbf{e}_n(\mathbf{x}) \,, \tag{12}$$

we can easily calculate projection $P(G)$ by zeroing coefficients g_n corresponding to irrotational modes. Using this expansion and the fact that e_i are linearly independent, we can deduce from (11) a set of ordinary differential equations for the unknown coefficients a_n:

$$\dot{a}_n = -\lambda_n a_n + g_n \,. \tag{13}$$

The set of equations (13) constitutes the set of discrete equations we were looking for. Note that this method requires a number of collocation points $\{\mathbf{x}_i\}$ that matches the dimension of the functional basis.

3.2. Nonlinear terms

The main difficulty in solving (13) lies in calculating coefficients g_n. In standard spectral methods, this is done by transforming the velocity field back to the physical space, calculating $\mathbf{u}\otimes\mathbf{u}$ at every discretisation point, transforming the result of this operation forward and calculating derivatives using properties of the basis elements. Unlike for Fourier modes, no simple analytical formulae express the spatial derivatives of basis vectors in terms of these vectors. We therefore have to first calculate the values of all spatial derivatives at the discretisation points, then combine them to calculate the non-linear terms and finally calculate the spectral expansion of the result. An additional obstacle is that no fast transform is available to calculate a_n for the basis we are using. Moreover, even in the relatively simple configuration considered here, the eigenvectors used as a basis are not orthogonal to each other. Therefore the spectral decomposition cannot be obtained by calculating the scalar product of the decomposed field with the elements of the basis.[1] Projection would require the knowledge of the eigenvectors of the adjoint operator which cannot be readily obtained. The reverse transformation consists of the reconstruction of values of the vector field at a given set of discretisation points assuming its spectral expansion is known. By contrast to the forward transform, it is straightforward to calculate, since the values of the basis functions are known at each of the discretisation points. These values can be calculated once at the beginning of calculations and used later in an array format at every time step. This speeds up the calculations at the cost of an increased memory usage. On this grounds, the forward transformation (calculation of a spectral decomposition of a vector field which is known at the set of discrete points in space) can be formulated as a set of linear equations for unknown spectral components:

$$g_n\mathbf{e}_n(\mathbf{x}_i) = G(\mathbf{u}(\mathbf{x}_i))\,. \tag{14}$$

As the elements of matrix $\mathbf{e}_n(\mathbf{x}_i)$ in this set of equation do not change during a single numerical run, it is worth performing the *LU* decomposition of the corresponding matrix at the beginning of calculations and later use it to efficiently find the spectral decompositions.

For the above method to converge in the limit of $n\to\infty$, the space spanned by the basis $\mathbf{e}_n$ has to include the images of all divergent free fields $\mathbf{u}(\mathbf{x})$ by the non-linear operator G. However, the eigenmodes of $\mathcal{D}_{Ha}$ given by [7] only span the divergence free subspace of all functions satisfying the boundary conditions of the problem. Therefore (14) is expressed using both sets of modes even though only those coefficients g_n corresponding to the solenoidal modes are actually calculated.

3.3. Using Fourier transform in XY directions

The technique presented so far is quite general, and can be used for any problem, as long as the solutions to the eigenvalue problem for the underlying operator can be found and divided into two disjoint subsets: irrotational and solenoidal. However, its usage for three-dimensional calculations would be impractical with current computational resources. For the case of low *Rm* channel flows with transverse magnetic fields this difficulty can be overcome due to special form of eigenmodes. As seen in Appendix A, the eigenmodes of $\mathcal{D}_{Ha}$ can be factorised as the product of two scalar functions of x and y respectively, and a vector function of z. Moreover, the functions of x and y consist of Fourier modes for which wavenumbers in x, y directions are integer multiples of 2π. Therefore the set of eigenmodes can be enumerated by a tuple of three integer numbers (n_x, n_y, n_z) (where $n_z = 6q + j$) and for every mode we can define the vector function $\mathbf{E}_{n_x,n_y,n_z}(z)$ such every mode $\mathbf{e}_{\{k_x,k_y,q,j\}}$ takes the form

$$\mathbf{e}_{\{k_x,k_y,q,j\}} = \mathbf{E}_{n_x,n_y,n_z}(z)\exp\left(i2\pi n_x x + i2\pi n_y y\right), \tag{15}$$

where $k_x = 2\pi n_x$ and $k_y = 2\pi n_y$. We can thus speed up the transformation from physical to spectral space by first performing two-dimensional Fast Fourier Transform in the x–y direction. This brings the transformed field under the form:

$$G(\mathbf{u}(x_i, y_i, z_i) = \sum_{n_x,n_y} \mathbf{A}_{n_x,n_y}(z_i)\exp\left(i2\pi n_x x_i + i2\pi n_y y_i\right), \tag{16}$$

where $\mathbf{A}_{n_x,n_y}$ is the complex amplitude of Fourier mode $(2\pi n_x, 2\pi n_y)$. Then, following the technique described in 3.2, for every value of (n_x, n_y) we find the set of spectral coefficients $\{g_{n_x,n_y,n_z}\}$ by solving a set of equations

$$\sum_{n_z} g_{n_x,n_y,n_z}\mathbf{E}_{n_x n_y n_z}(z_i) = \mathbf{A}_{n_x,n_y}(z_i)\,. \tag{17}$$

The reverse transformation is speeded up in a similar fashion.

Using the Fast Fourier transform in x–y planes imposes the distribution of discretisation points in these planes: they have to form a regular rectangular grid. We denote its dimensions as $N_x \times N_y$. In our simulations we also use a uniform grid of dimension N_z in the z direction. In order for the set of equations (14) to have a unique solution the number of modes used during the spectral decomposition has to be equal to N_z, while the total number of independent modes used in the calculations is $N = N_x N_y N_z$.

[1] It is worth mentioning, that even if the aforementioned basis, known analytically, was orthogonal for scalar product $\langle\cdot|\cdot\rangle$, we would still be facing the same problem with its discrete counterpart: in general it is not possible to find a set of discretisation points such that the associated discrete functional basis is orthogonal.

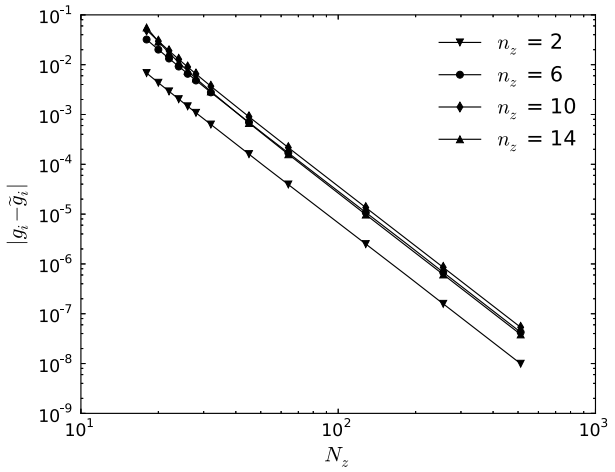

Fig. 2. The relative error in determination of $g_{16,0,n_z,4}$ for $n_z = 1, 3, 5, 7$ as a function of grid size in the z direction. The decomposed field is $(\mathbf{u}\cdot\nabla)\mathbf{u}$, where $\mathbf{u}$ is the single eigenmode $\mathbf{e}_{8,0,7,3}$ for $Ha = 1$, normalised in such a way that its amplitude is 1.

3.4. Estimation of number of required discretisation points in z directions

The technique described above has the advantage that the obtained spectral decomposition reproduces exactly the physical fields on the given set of discretisation points. Therefore momentum and energy are conserved by this procedure. However, the obtained spectral coefficients g_n are different from the exact ones $\widetilde{g}_n$, which would be the result of decomposition of the same vector field in a space of infinite dimension spanned by all eigenvectors. $|\widetilde{g}_n - g_n|$ is the so-called aliasing error. In spectral methods based on standard functional bases (Fourier or orthogonal polynomials), there are known procedures to correct this error. They all rely on the fact that the spectral decomposition of non-linear terms can be calculated analytically for the elements of the functional basis. Unfortunately, in our case these are only known in the x and y directions, where we adopt the $3/2N$ rule for de-aliasing [11]. In the z direction we adapt this procedure by performing the discrete transformation with a number of modes N larger than the one strictly required by the system's dynamics, N_D (The latter is of the order of the attractor dimension of the dynamical system underlying the given problem [3]). After every evaluation of the spectral decomposition, the coefficients corresponding to these additional modes are padded with zeros. In other words, the set of equations (14) is expanded over N modes, but only the first N_D coefficients are calculated. Since the decomposition over N modes is more precise than that over N_D modes but still not exact, this procedure does reduce the de-aliasing error but does not remove it completely. Note that the number of discretisation points is then N, not N_D.

We have evaluated the residual aliasing error on a number of examples and reported some of them in Figs. 3 and 2. These show the relative error $\epsilon_a = |g_n - \widetilde{g}_n|/g_n$ for several values of n as a function of the number of modes used in decomposition in the z direction N_z. For the purpose of this test, we built the non-linear terms $(\mathbf{u}\cdot\nabla)\mathbf{u}$ out of the single mode $\mathbf{e}_{8,0,7,3}$, which we found to be representative of the behaviour observed using other modes.

Two regimes can be distinguished. For low values of Ha, the relative error in g_n drops monotonically for all plotted values of N_z (see Fig. 2). This is because the smallest scales in the decomposed field result from its oscillatory part, which physically represent small vortices in the bulk of the flow, the size of which is practically independent of Ha (see [7]). The picture looks qualitatively different at high Hartmann numbers (see Fig. 3). In this case, the smallest structures in the decomposed velocity field are the Hartmann layers. Up to $N_z \sim Ha$, the number of discretisation points is insufficient to resolve them. Consequently, the de-aliasing errors is high and remains more or less constant. Above this value of N_z, the Hartmann layer is correctly resolved and the error introduced by spectral decomposition starts to drop, roughly following a power law of the form $\epsilon_a \sim N_z^{-\alpha}$, with $\alpha \approx 4$. We use this approach in every calculation to determine the number of discretisation points required in the z direction in order to keep the de-aliasing error below the specified level of accuracy ϵ: for a given value of N_D, this is done by constructing the non-linear term

$$\mathbf{e}_{N_x/2,N_y/2,N_D/6,j}\cdot\nabla\mathbf{e}_{N_x/2,N_y/2,N_D/6,j}\,,$$

for every $j = 1, 2, 3, 4, 5, 6$, calculating its spectral decomposition for different values of N, and pickup the smallest value N for which the relative error ϵ_a is below ϵ. Since modes of highest index are expected to generate the largest error, this ensures that de-aliasing remains below the specified precision.

3.5. Parallelisation

The code has been parallelised for memory distribution systems using the domain decomposition approach. Since in order to calculate Fourier transform in the x and y direction we are using the FFTW library [12], we adopted the strategy implemented therein to distribute arrays between different computational nodes. Its principle is that every three-dimensional

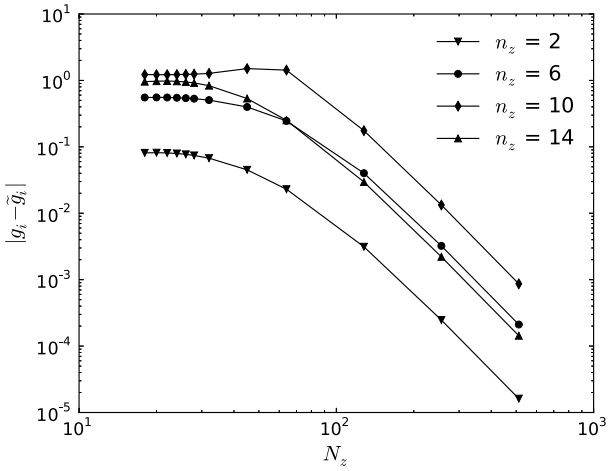

Fig. 3. The relative error in determination of $g_{16,0,n_z,4}$ for $n_z = 1, 3, 5, 17$ as a function of grid size in the z direction. The decomposed field is $(\mathbf{u}\cdot\nabla)\mathbf{u}$, where $\mathbf{u}$ is the single eigenmode $\mathbf{e}_{8,0,7,3}$ for $Ha = 100$, normalised in such a way that its amplitude is 1.

array representing a component of velocity as a function of $\mathbf{x}$ or their spectral decomposition (in spectral representation) is divided into slabs orthogonal to their first dimension. In our problem, this corresponds to a division of computational domain into slabs along planes $x = const$ and $k_x = const$ in physical and spectral spaces respectively. Every computational core is assigned such a single block. Additional speedup is gained from the ability of the library to perform multiple transforms at once, of interleaved data. This makes it possible to decrease the cost of inter-node communication by calculating multiple 2D FFT transformations for different values of z simultaneously. Further speed-up can be obtained by parallelising the matrix by vector multiplications during the calculation of spectral expansions.

3.6. Time discretisation

To numerically solve equation set (13) of ODEs in time, we use an integrating factor technique (see [11]), and rewrite eqs. (13) as:

$$\frac{d}{dt}[e^{\lambda_n t} a_n] = -e^{\lambda_n t} g_n \,. \tag{18}$$

We then implement the Euler approximation to provide solution a_n^{k+1} at instant t_{k+1} in terms of solutions $\mathbf{a}_n^k$ at previous time step $t_k = t_{k+1} - \Delta t$

$$a_n^{k+1} = -e^{\lambda_n \Delta t}[a_n^k - \Delta t\, g_n(\mathbf{a}^n)] \,. \tag{19}$$

The value of Δt was chosen at every time step according to the equation:

$$\Delta t = 1.2 \min_n \left| \frac{a_n}{g_n(\mathbf{a}^n)} \right| .$$

4. Comparison with DNS

4.1. Reference numerical setup based on OpenFOAM

To validate the present numerical scheme we compared the results it produces with those of three-dimensional, time-dependent direct numerical simulations performed with a code based on the open source framework OpenFOAM, on test cases of freely decaying MHD turbulence. OpenFOAM is based on the finite volume approach and uses a co-located grid. Our MHD code is based on it, and implements the set of low Rm MHD equations (1)–(4) using second order spatial discretisation and second order, implicit time scheme. The equations are solved segregated and the PISO algorithm is used to handle the velocity-pressure coupling. The conservation of charge is ensured by calculating current density and Lorentz force following the approach proposed by [9]. The details of its implementation in OpenFOAM and its validation are described by [10]. The spectral methods described in the previous sections were implemented by modifying the spectral code TARANG developed by [13].

Our numerical domain was a cube of dimension L divided uniformly into N cells in every direction. This configuration is a fair representation of the experiment conducted in [14], in which MHD turbulence is electrically driven in a cubic container pervaded by a transverse magnetic field. In order to calculate correctly the electric current density in Hartman layers we always resolve each of them with at least three computational cells in the z direction, as in [10]. Therefore the Hartman

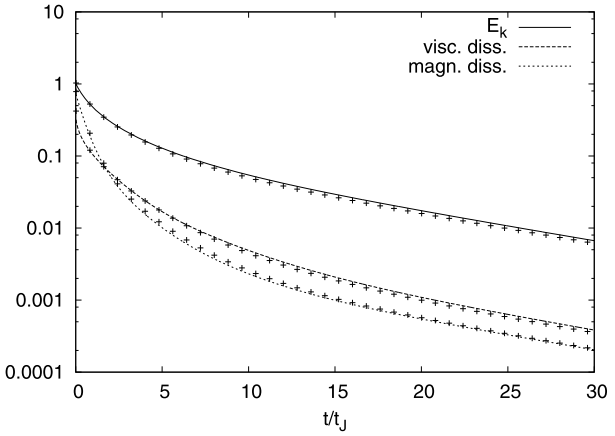

Fig. 4. Total kinetic energy (normalised by its initial value) and viscous and magnetic dissipation rates (normalised by initial kinetic energy divided by t_J) in test case with $Ha = 56$ *vs.* time normalised by the Joule time. The lines and points respectively represent the results obtained with finite volume and spectral codes.

number is connected to the resolution by $N = Ha/6$. Following the DNS of decaying MHD turbulence in a three-dimensional periodic domain by [15], the initial conditions consist of a random Gaussian velocity field with $u_i(k) \sim \exp[(-k/k_p)^2]$ where $k_p = 4\pi/L$. This corresponds to the energy spectrum $E \sim k^4 \exp[-2(k/k_p)^2]$. For this choice of initial velocity field, the integral scale of turbulent motions is given by $l = \sqrt{2\pi}/k_p$. The velocity spectrum was normalised in such a way that cell sizes correspond to $l_K/1.4$ where $l_K = l\,Re^{-3/4}$ is the Kolmogorov length scale and the Reynolds number in its definition $Re = u'l/\nu$ is based on l and velocity $u' = u(k = k_p)$. With this choice, the Reynolds number and the Hartmann number are linked by $Re = 0.13Ha^{4/3}$. This strategy allows us to calculate the most intense flow possible whilst minimising mesh-induced numerical errors at a given mesh size, since the mesh is always uniform.

4.2. Freely decaying turbulence

For the reference case, we have chosen $Ha = 56$, a value within reach of a traditional code such as OpenFOAM. Adopting the procedure presented in previous subsection for OpenFOAM calculations we use $N_x = N_y = N_z = 170$ number of points in every direction and initial conditions characterised by Reynolds number $Re = 28$. We have followed the evolution of the initial conditions up to a time corresponding to $30\,t_J$, where $t_J = \sigma B^2/\rho$ is the timescale of Joule dissipation. We have also performed a shorter calculation up to $t = t_J$ with twice this resolution in every direction. The difference between the magnetic and viscous dissipation rates were smaller then 1 per cent, so it is safe to consider that the run in standard resolution is fully converged.

For the corresponding spectral calculations we use a resolution 1.5 times higher ($N_x = N_y = N_z = 256$) in order to reduce the de-aliasing errors. The initial conditions were chosen in such a way that their values on grid points of grid $N_x = N_y = N_z = 170$ was identical to the initial conditions used in the calculations with OpenFOAM.

Fig. 4 shows the evolution of the normalised global kinetic energy, the viscous and magnetic dissipation rates *vs.* time normalised by the Joule time. These quantities were respectively calculated as:

$$E(t) = \int \frac{1}{2}\mathbf{u}^2 \mathrm{d}V\,, \quad \epsilon_\nu = \int \frac{1}{2}\sum_{ij}\sigma_{ij}\sigma_{ij}\mathrm{d}V\,, \quad \epsilon_M = \int \sigma \mathbf{j}^2 \mathrm{d}V\,, \tag{20}$$

where

$$\sigma_{ij} = \nu\left(\frac{\partial u_i}{\partial x_j} + \frac{\partial u_j}{\partial x_i}\right) \tag{21}$$

is the viscous stress tensor. The normalisation factor corresponds to the initial value of kinetic energy for E and to the initial value of kinetic energy multiplied by the Joule time for dissipation rates. All presented quantities exhibit quantitatively and qualitatively the same agreement in both codes. The spectral code exhibits a slightly smaller values of viscous dissipation then the finite volume code and slightly higher magnetic dissipation. The relative difference in the total kinetic energy after 30 Joule times is below 10%, the spectral code being overall the more dissipative one.

We also compared the power spectral densities for spectral parameter $\sqrt{-\lambda}$ resulting from both codes at $t = 30\tau_J$ ($\sqrt{-\lambda}$ is the equivalent of the wavenumber in Fourier based spectral decomposition [7]). To this aim we expanded both numerical solutions onto the set of least dissipative modes used in the spectral simulation, following the procedure described in Section 3 and compared the kinetic energies corresponding to each value of λ. The results are presented in Fig. 5. Both codes produce quantitatively similar results. Qualitatively, the spectral code seems to be more dissipative, and as a result,

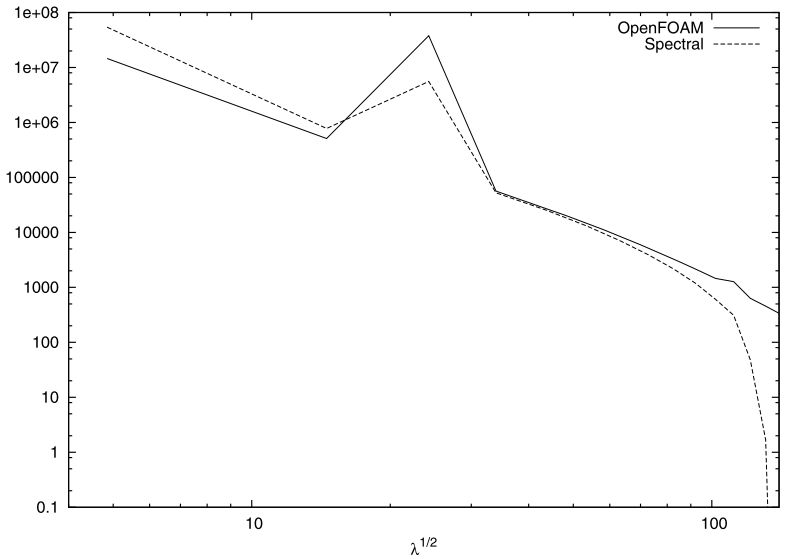

Fig. 5. The energy contained in modes with given value of λ for case with $Ha = 56$ after $t = 30\,t_J$. The solid line represents calculations performed with OpenFOAM while the dashed line shows the results obtained with the spectral code.

more energy is concentrated in the largest scales at the expense of the large-intermediate ones. For mid to small scales up to $|\lambda| \sim 80$ both codes agree well. The difference in the smallest scales can be explained as follows. The computational domain in physical space is rectangular, so it is in the (k_x, k_y, κ_z) space. Since curves $\lambda(k_x, k_y, \kappa_z) = const$ are a family of cardioids, this space only includes full λ-shells up to $|\lambda| \approx 80$. On these grounds the $\sqrt{\lambda}$-PSD spectra is a physically meaningful representation of the solution up to $|\lambda| = 80$.

4.3. Simulations at intermediate Ha

In the previous section we showed that the results obtained with the new spectral approach were able to reproduce those obtained with using the finite volume technique, in a case accessible to both methods. For the purpose of this test, we used in our spectral calculations and an effective number of modes N_D (those which were not padded with zeros in the de-aliasing procedure), which was the same as the number of grid cells in calculations performed with OpenFOAM. This imposed to choose a rather low Hartmann number so as to keep the computational cost low in both methods. It is, however, for flow at high *Ha*, that our new approach can potentially offer computational savings, because the theoretically predicted number of degrees of freedom is much lower than the number of grid points required in the mesh used in the finite volume method (or in a classical spectral method). The full calculations of decaying or forced MHD turbulence at high *Ha* are beyond scope of this contribution, as they would require a full scale parallelisation of our code, which is not yet implemented. Our main purpose is to present an implementation of our new spectral method and show that it gives accurate results. Nevertheless, we shall still demonstrate its potential for calculations at higher values of *Ha*. To this end, we used a different approach to examine the computational savings offered by this new technique. We start with initial conditions determined as in the previous section for $Ha = 108$. The flow is then evolved for a period of $0.3\,t_J$ to erase the trace of the initial non-MHD flow. At this instant we removed from the resulting velocity field all contributions from modes with $|\lambda| > |\lambda_{\max}| = 10^4$. This value is located just behind a sharp drop in PSD, which is an early indication of its relevance as an estimate for the smallest scales. Subsequently we let the flow evolve for another $0.3\,t_J$. Then we examined the power density λ-spectrum of the resulting velocity field and compared it to that at $t = 0.3\,t_J$, seeking in particular if energy had leaked into regions of the spectrum where $|\lambda| > |\lambda_{\max}|$. The results are presented in Fig. 6 We see that the evolution of the spectrum was not significantly influenced. This indicates that the evolution of the flow is sufficiently well described by the modes with $|\lambda| \leq |\lambda_{\max}|$, and our method does carry the ability to resolve high *Ha* flows with the limited number of modes.

4.4. Simulations at high Ha

Validation at high Hartmann number is less straightforward. Our setup with OpenFOAM does not allow us to calculate decaying turbulence at very high Hartmann number. Usually, Hartmann flow is the classical validation test for MHD flows and it can be used at very high Hartmann number. The specificity of our method, however, is to provide *by construction* a solution which is exact to machine precision for any problem where the non-linear terms are zero. Consequently, it can resolve the Hartmann flow "exactly" at arbitrarily high Hartmann number at practically no computational cost, without involving the collocation steps. Therefore, such a solution does not provide a realistic measure of the code precision, which is determined by the way in which the non-linear terms are handled.

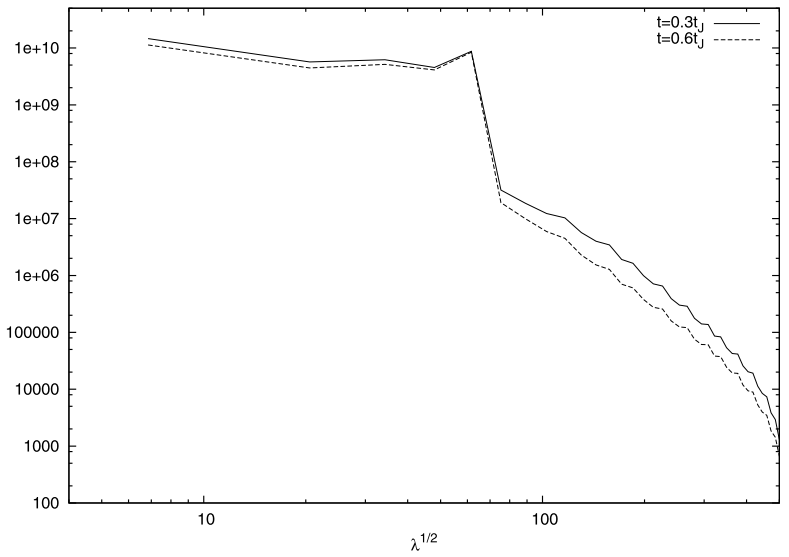

Fig. 6. The energy contained in modes with given value of λ for case with $Ha = 56$. The solid line shows λ-spectra at $t = 0.3$ Joule times. Then all the modes with $\lambda > 100$ were padded to zero and the flow was evolved for another 0.3 Joule times. The final λ spectrum is represented by a dashed line.

In the absence of an analytical solution to non-linear MHD flow problem in the channel configuration, we were faced with the dilemma of having to validate our code in a regime which no other method can reach. To overcome this difficulty, we checked asymptotic convergence of global quantities at high Hartmann numbers. In the limit $Ha \to \infty$, the turbulence becomes quasi-two-dimensional and in the later stages of the decay, energy should follow a near exponential curve of the scale of the Hartmann friction time t_{Ha}. In that regime the flow can be described by two-dimensional Sommeria and Moreau model, to a precision (Ha^{-1}, N^{-1}) [16]:

$$\frac{\partial \mathbf{u_{2D}}}{\partial t} + (\mathbf{u_{2D}} \cdot \nabla)\mathbf{u_{2D}} = -\frac{1}{\rho}\nabla p + \nu \Delta \mathbf{u_{2D}} - \frac{1}{t_{Ha}}\mathbf{u_{2D}}\,, \tag{22}$$

$$\nabla \cdot \mathbf{u_{2D}} = 0\,, \tag{23}$$

where $\mathbf{u_{2D}}(t, x, y)$ is the velocity field averaged along direction of the imposed magnetic field and

$$t_{Ha} = \frac{1}{2}\frac{L^2}{\nu Ha}\,. \tag{24}$$

We assumed periodic boundary conditions in all two directions. If the initial conditions are in the form:

$$u^x_{2D}(t = 0) = V_{2D} \sin kx \cos ky, \tag{25}$$

$$u^y_{2D}(t = 0) = -V_{2D} \cos kx \sin ky, \tag{26}$$

it is easy to verify that the solution of (22), (23) is:

$$\mathbf{u_{2D}}(t, x, y) = \mathbf{u_{2D}}(t = 0, x, y) \exp[-(1/t_{Ha} + \nu k^2)t]. \tag{27}$$

To verify our code against the 2D approximation we performed a set of two simulations with $Ha = 448$ and $Ha = 896$. The velocity field was initialised with:

$$\mathbf{u}(t = 0) = V\,\mathbf{e}_{k_x,k_y,0,Ss}, \tag{28}$$

where $k_x = k_y = 2\pi/L$. The amplitude V was chosen in such a way as to be equivalent to $V_{2D} = 1250\nu/L$. Fig. 7 shows the evolution of normalised global kinetic energy. In both cases the decay of the energy closely follows the analytical prediction given by eq. (27). We interpret the slightly larger dissipation rate in the $3D$ calculations as the results of three-dimensionality induced in the bulk by non-linear terms, which is neglected in 2D approximation. The lower discrepancy to the analytical solution at high Ha tends to confirm this interpretation. Since in a quasi-two-dimensional configuration, practically all the Joule and viscous dissipation takes place in the Hartmann layers, this test provides very good evidence that these layers are very well resolved by our method, even at very high Hartmann number.

5. Computational cost

The cost of pseudospectral codes based on FFT technique scales as $N_x N_y N_z \log(N_x N_y N_z)$. In DNS calculations, N_i should be of the order of Reynolds number $Re^{3/4}$ each. Moreover, to obtain physically meaningful results, it is necessary to resolve

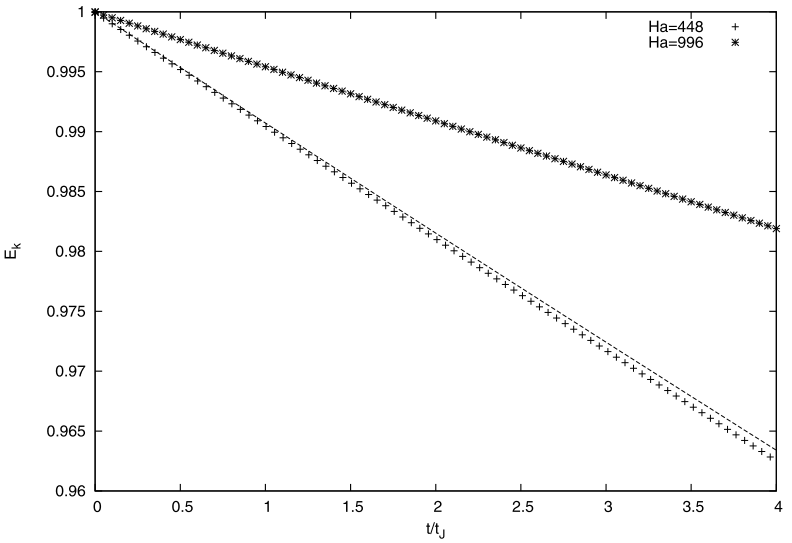

Fig. 7. Total kinetic energy (normalised by its initial value) in test cases with quasi-2D initial conditions *vs.* time normalised by the Joule time for $Ha = 448$ and $Ha = 896$. The points represents the results of the 3D spectral code, while the lines show the analytical solution to 2D approximation.

the Hartmann layer in the z direction. N_z should therefore be at least of the order of $Ha^{1/2}$. For large Hartmann number calculations, the computational cost of the FFT based code thus scales at least as $\sim Re^{3/2}Ha^{1/2}\log(ReHa)$. As explained in Section 3.3, the spectral decomposition described in Section 3.2 is only used to treat the z-dependence while the spectral decomposition in x–y directions can be performed with FFT. The computational cost in this case scales as $\sim N_x N_y N_z^2$. Using the estimation for the number of degrees of freedom in low Rm MHD flows from [17,3]: $N_{x,y} \sim Re^{1/2}$, $N_z \sim Re/Ha$. In Section 3.4, however, we found that it is still necessary to have $N_z \sim Ha$ to calculate accurate spectral coefficients with small errors. Nevertheless, we only need to calculate Re^2/Ha spectral coefficients, as the rest of them will be dissipated over very short timescales and are not physically meaningful. Therefore the total computational cost of the proposed scheme scales as $\sim Re^2$. The proposed method has the potential to significantly reduce the computational cost incurred by traditional ones in the regime of high values of Ha, as its computational cost does not depend on the intensity of the magnetic field, which is a limiting factor for traditional methods. Theoretically, there is room for additional improvement as the number of degrees of freedom in low Rm MHD flows is inversely proportional to Ha. However, this would require an alternative approach for the treatment of the non-linear terms.

6. Conclusions

We have presented a novel model method to simulate MHD flows in channel configurations. It is based on using the sequence of least dissipative eigenmodes from the dissipation operator instead of the traditional Fourier or Tchebychev basis. The advantage is that these modes show physical properties of the actual MHD flow. Consequently, the basis requires a smaller number of modes. On the other hand, they lack advantageous properties of usual bases, such as orthogonality and the existence of fast transforms, which are heavily relied upon in standard spectral methods. We have put forward an approach to overcome this difficulties and were able to construct a useful numerical scheme based on this alternative modes. We tested this new method by comparing its ability to calculate the freely decaying MHD turbulence in a channel to that of a finite volume code. We obtained very good agreement between the two codes both in terms of global quantities such as energy dissipation rates and in terms of the resulting energy spectra. We also verified the potential of the new scheme to efficiently resolve flows in the presence of high magnetic fields with a limited number of modes. As a last test we verified that the computations at high Hartmann numbers approached the two-dimensional limit. Since, in this state, dissipation occurs exclusively in the Hartmann layers, this provides a good evidence that these are accurately resolved even when the bulk of the flow retains a complex structure.

Application of this technique to other problems with the code presented in this paper can be straightforward provided that

1. Eigenmodes of the linear part of the Navier–Stokes equation are known either analytically or numerically,
2. These modes can be easily separated in families of curl-free and solenoidal modes,
3. The x and y dependence is still represented by Fourier modes.

MHD channel flows are the simplest example: the basis of eigenmodes presented in appendix indeed includes modes with a non-zero flow rate. Forcing energy into them presents no numerical novelty compared to the work presented here.

Other examples can require a new basis: for example, if the boundary conditions at $z=-1$ and $z=1$ are changed (for example, slip free, electrically conducting boundary conditions, etc.). In this case, it is straightforward to replace the basis used in this paper by the new basis. Further examples, keeping the geometry of this paper, involve arbitrarily changing the direction of the magnetic field (see [18] for a derivation of the basis of functions in the case of a spanwise magnetic field), or flows with a background rotation of arbitrary direction. Pipe flows (MHD or with background rotation) also satisfy all conditions (if x and y are taken in the axial and azimuthal directions). However, their treatment would require expressing the non-linear terms in cylindrical coordinates. Simulating MHD flows using the full MHD equations at arbitrary values of the magnetic Reynolds number would require extending the existing treatment of the nonlinear terms in the Navier–Stokes equation to the bi-linear terms of the induction equation.

The method is still applicable to cases where Fourier dependence is lost either along x or y or both. However, its computational cost would then considerably increase and more extensive modifications would have to be built into the code. In particular, the *LU* decomposition could become impractical to calculate the nonlinear terms. Duct flows, or flows in non-uniform magnetic fields fall into this category. In all these examples, the usefulness of the method must still be measured through its ability to simulate the flow exactly using a reduced number of modes. For example, flows with background rotation are a particularly good candidates since, as Low-Rm MHD flows, very thin boundary layers, called Ekman layers [19], appear along walls non-parallel to the background rotation.

Acknowledgements

The authors gratefully acknowledge financial support of the Leverhulme Trust (Grant F00/732J). The authors are also grateful to Professor Mahendra Verma, for making the TARANG code available to them and for fruitful discussions around the ideas presented in this paper. Finally, the authors would like to express their gratitude to Antoine Huber for his work in the numerical simulations carried out with OpenFOAM.

Appendix A. Analytical expression of the eigenmodes of $\mathcal{D}_{Ha}$

Ref. [7] provides solutions to divergence free eigenvalue problem for operator (6). Every eigenvalue can be identified by a tuple $(\mathbf{k}_\perp, \kappa_z, \mu)$ where $\mathbf{k}_\perp = (2\pi n_x/L, 2\pi n_y/L), n_x, n_y \in \mathbb{Z}$ is a wave vector in a plane perpendicular to the magnetic fields, $\kappa_z \in \mathbb{R}_+$ is a wave number in z direction and $\mu \in \mathbb{R}_+$ is an inverse of the thickness of boundary layer present in the given mode The eigenvalues λ are given by dispersion relation:

$$\lambda = -(k_x^2 + k_y^2 - K) + Ha^2 \frac{K}{k_x^2 + k_y^2 - K}, \tag{A.1}$$

where for a given λ K can take values $-\kappa_z^2$ and μ^2. The numbers κ_z and μ are related by equation:

$$\kappa_z^2 \mu^2 - k_\perp^2 (k_\perp^2 - \mu^2 + \kappa_z^2 + Ha^2) = 0. \tag{A.2}$$

A.1. Divergence-free modes

Divergence free eigenvectors can be divided into three subgroups.

A.1.1. Orr–Sommerfeld modes

These are in turn divided based on whether velocity component perpendicular to $\mathbf{e}_z$ is symmetric or antisymmetric in z.
Symmetric modes:

$$\mathbf{e}_\lambda^{OSs} = \left\{ i\kappa_z \cos\kappa_z \mathbf{k}_\perp \left(\frac{\cos(\kappa_z z)}{\cos(\kappa_z)} - \frac{\cosh(\mu z)}{\cosh(\mu)} \right) + k_\perp^2 \sin\kappa_z \mathbf{e}_z \left(\frac{\sin(\kappa_z z)}{\sin(\kappa_z)} - \frac{\sinh(\mu z)}{\sinh(\mu)} \right) \right\} \exp(i\mathbf{k}_\perp \cdot \mathbf{r}_\perp), \tag{A.3}$$

with κ_z and μ satisfying:

$$\kappa_z \tanh(\mu) - \mu \tan(\kappa_z) = 0. \tag{A.4}$$

Antisymmetric modes

$$\mathbf{e}_\lambda^{OSa} = \left\{ i\kappa_z \sin\kappa_z \mathbf{k}_\perp \left(\frac{\sin(\kappa_z z)}{\sin(\kappa_z)} - \frac{\sinh(\mu z)}{\sinh(\mu)} \right) - k_\perp^2 \cos\kappa_z \mathbf{e}_z \left(\frac{\cos(\kappa_z z)}{\cos(\kappa_z)} - \frac{\cosh(\mu z)}{\cosh(\mu)} \right) \right\} \exp(i\mathbf{k}_\perp \cdot \mathbf{r}_\perp). \tag{A.5}$$

with κ_z and μ satisfying:

$$\kappa_z \tan(\kappa_z) + \mu \tanh(\mu) = 0. \tag{A.6}$$

A.1.2. Squire modes

Symmetric modes:

$$\mathbf{e}_\lambda^{Ss} = \mathbf{k}_\perp \times \mathbf{e}_z \left(\frac{\cos(\kappa_z z)}{\cos(\kappa_z)} - \frac{\cosh(\mu z)}{\cosh(\mu)} \right) \exp(i\mathbf{k}_\perp \cdot \mathbf{r}_\perp), \tag{A.7}$$

with κ_z and μ satisfying:

$$S\tan(\kappa_z) + M\tanh(\mu) = 0. \tag{A.8}$$

Antisymmetric modes

$$\mathbf{e}_\lambda^{Sa} = \mathbf{k}_\perp \times \mathbf{e}_z \left(\frac{\sin(\kappa_z z)}{\sin(\kappa_z)} - \frac{\sinh(\mu z)}{\sinh(\mu)} \right) \exp(i\mathbf{k}_\perp \cdot \mathbf{r}_\perp), \tag{A.9}$$

with κ_z and μ satisfying:

$$S\tanh(\mu) - M\tan(\kappa_z) = 0. \tag{A.10}$$

Quantities S and M are defined by relations:

$$S = \kappa_z \left(k_\perp^2 - \mu^2 \right) \quad \text{and} \quad M = \mu \left(k_\perp^2 + \kappa_z^2 \right).$$

A.1.3. Modes with $\mathbf{k}_\perp = 0$

These are the modes in which the velocity is function of the z coordinate only. They are omitted in [7] and we had to derive them independently. Because of the requirement that $\mathbf{u}$ is divergence free and the non-slip boundary conditions at $z = \pm 1$, u_z has to vanish everywhere. Moreover $\nabla \cdot (\sigma \mathbf{u} \times \mathbf{B}) = 0$ for this modes. Additionally $\sigma \mathbf{u} \times \mathbf{B}$ satisfies boundary conditions imposed on $\mathbf{j}$. Therefore in this case the electric potential vanishes in the whole of the domain for the considered modes and the electric current density is given by the expression:

$$\mathbf{j} = \sigma \mathbf{u} \times \mathbf{B}.$$

Therefore the eigenvalue problem in this case reduces in dimensionless form to:

$$\Delta \mathbf{u} = (\lambda + Ha^2)\mathbf{u},$$

$$\mathbf{u}|_{z=\pm 1} = 0.$$

Again the modes can be divided into symmetric and antisymmetric ones.

Symmetric modes:

$$\mathbf{e}_{\kappa_z}^i = \cos(\kappa_z z)\mathbf{e}_i, \qquad i = x, y, \tag{A.11}$$

where $\kappa_z = \pi/2q$ and q is an odd natural number.

Antisymmetric modes:

$$\mathbf{e}_{\kappa_z}^i = \sin(\kappa_z z)\mathbf{e}_i, \qquad i = x, y, \tag{A.12}$$

where $\kappa_z = \pi/2q$ and q is an even natural number.

A.2. Irrotational modes

Our approach required also derivation of curl-free eigenvectors. They are in one to one relation with Orr–Sommerfeld modes.

Symmetric modes:

$$\mathbf{e}^{Cs}(\lambda) = \left\{ \cos\kappa_z \mathbf{k}_\perp \left(\frac{\cos(\kappa_z z)}{\cos(\kappa_z)} - \frac{\cosh(\mu)}{\cosh(\mu)} \right) + i\kappa_z \sin\kappa_z \mathbf{e}_z \left(\frac{\sin(\kappa_z z)}{\sin(\kappa_z)} - \frac{\sinh(\mu z)}{\sinh(\mu)} \right) \right\} \exp(i\mathbf{k}_\perp \cdot \mathbf{r}_\perp), \tag{A.13}$$

with κ_z and μ satisfying (A.6).

Antisymmetric modes:

$$\mathbf{e}^{Ca}(\lambda) = \left\{ -\sin\kappa_z \mathbf{k}_\perp \left(\frac{\sin(\kappa_z z)}{\sin(\kappa_z)} - \frac{\sinh(\mu z)}{\sinh(\mu)} \right) + i\kappa_z \cos\kappa_z \mathbf{e}_z \left(\frac{\cos(\kappa_z z)}{\cos(\kappa_z)} - \frac{\cosh(\mu z)}{\cosh(\mu)} \right) \right\} \exp(i\mathbf{k}_\perp \cdot \mathbf{r}_\perp), \tag{A.14}$$

with κ_z and μ satisfying (A.4).

Solutions to dispersion relations are such that for a given $\mathbf{k}_\perp$ and every $q \in \mathbb{N}$, there are six modes for which $\kappa_z \in [q\pi, (q+1)\pi]$.

A.3. Distribution of the modes

For a given $\mathbf{k}_\perp$ and every $q \in \mathbb{N}$ there are six modes with $\kappa_z \in [q\pi, (q+1)\pi]$. Therefore modes can be indexed by tuple $\{k_x, k_y, q, j\}$, where $j = 1, 2, 3, 4, 5, 6$ indicates correspondingly *OSs, OSa, Ss, Sa, Cs, Ca* modes.

References

[1] S. Smolentsev, L. Moreau, R. Buehler, C. Mistrangelo, MHD thermofluid issues of liquid-metal blankets: phenomena and advances, Fusion Eng. Des. (2010) 1196–1205.
[2] T. Boeck, D. Krasnov, E. Zienicke, Numerical study of turbulent magnetohydrodynamic channel flow, J. Fluid Mech. 572 (2007) 179–188.
[3] A. Pothérat, T. Alboussière, Bounds on the attractor dimension for low-*Rm* wall-bound MHD turbulence, Phys. Fluids (2006) 25102 (12 pages).
[4] O. Ladyzhenskaya, The Mathematical Theory of Viscous Imcompressible Flow, Gordon and Breach Science Publishers, New York, London, Paris, Montreux, Tokyo, Melbourne, 1968.
[5] P.W. Livermore, C.A. Jones, S.J. Worland, Spectral radial basis functions for full sphere computations, J. Comput. Phys. 227 (2007) 1209–1224.
[6] P.H. Roberts, Introduction to Magnetohydrodynamics, Longmans, 1967.
[7] V. Dymkou, A. Pothérat, Spectral methods based on the least dissipative modes for wall-bounded MHD turbulence, Theor. Comput. Fluid Dyn. 23 (6) (2009) 535–555.
[8] A. Pothérat, V. Dymkou, DNS of Low-*Rm* MHD turbulence based on the least dissipative modes, J. Fluid Mech. 655 (2010) 174–197.
[9] M.-J. Ni, R. Munipalli, N. Morley, P. Huang, M. Abdou, A current density conservative scheme for MHD flows at a low magnetic Reynolds number. Part I: On a rectangular collocated grid system, J. Comput. Phys. 227 (2007) 174–204.
[10] V. Dousset, A. Pothérat, Characterisation of the flow around a truncated cylinder in a duct in a spanwise magnetic field, J. Fluid Mech. 691 (2012) 341–367.
[11] C. Canuto, M. Hussaini, A. Quarteroni, T. Zang, Spectral Methods: Fundamentals in Single Domains, Springer-Verlag, 2006.
[12] M. Frigo Steven, G. Johnson, The design and implementation of FFTW3, in: Proceedings of the IEEE, 2005, pp. 216–231.
[13] M.K. Verma, A. Chatterjee, S. Reddy, R. Yadav, S. Paul, M. Chandra, R. Samtaney, Benchmarking and scaling studies of pseudo-spectral code Tarang for turbulence simulations, Pramāna 81 (4) (2013) 617–629.
[14] R. Klein, A. Pothérat, Appearance of three-dimensionality in wall bounded MHD flows, Phys. Rev. Lett. 104 (3) (2010).
[15] N. Okamoto, P.A. Davidson, Y.Y. Kaneda, On the decay of low-magnetic-Reynolds-number turbulence in an imposed magnetic field, J. Fluid Mech. 651 (2010) 295–318.
[16] J. Sommeria, R. Moreau, Why, how and when MHD turbulence becomes two-dimensional, J. Fluid Mech. 118 (1982) 507–518.
[17] A. Pothérat, T. Alboussière, Small scales and anisotropy in low-*Rm* MHD turbulence, Phys. Fluids (2003) 1370–1380.
[18] R. Low, A. Pothérat, Attractor dimension and least dissipative mode for MHD channel flows in a spanwise magnetic field, Phys. Rev. E 91 (2015) 053022.
[19] H. Greenspan, The Theory of Rotating Fluids, Cambridge Monographs on Mechanics and Applied Mathematics, Cambridge University Press, 1990.